JOURNAL OF COMPUTATIONAL PHYSICS 63, 247–267 (1986)

High-Order Spline Interpolations in the Particle Simulation

HIROTADE ABE, NATSUHIKO SAKAIRI,* AND RYOHEI ITATANI

Department of Electronics, Kyoto University, Kyoto 606, Japan

AND

HIDEO OKUDA

Plasma Physics Laboratory, Princeton University, Princeton, New Jersey 08544

Received July 4, 1984; revised April 16, 1985

In the conventional plasma simulation models using particles, in which the total momentum is conserved, the total energy is not conserved due to nonuniformity of space caused by the spatial grids. The grid spacing has been severely limited of order of the Debye length. It is found that the use of the high-order spline spatial interpolation removes this limit without a significant increase of the computation and complexity of the algorithm in the system that only the long-wavelength, collective phenomena are important. The theoretical analysis of the total energy is improved compared with the previous work and its scaling law is related to the so-called aliasing error explicitly. The coefficient η introduced previously is referred as the model index and is used again as a measure of the accuracy of the models for the energy conservation.

I. INTRODUCTION

In the conventional plasma simulation using particles, the use of a grid associated with the spatial interpolation is inevitable for the practical runs using the present digital computer, because the number of the particles used is so large. Some simple models such as Nearest Grid Point (NGP) [1], Cloud-in-Cell or Particle-in-Cell (CIC–PIC) [2, 3, 4] and dipole expansion and Subtracted Dipole (SUD) [5] have been commonly used.

It is well known that the applicability of the particle simulation using these simple spatial interpolations has been limited severely when the Debye length is shorter compared with the grid size [13], while there have been several attempts to reduce the restrictions [6, 7], more efforts may be necessary for the wider application to various problems of physics and technology. Here, we review the origin of the

* Present address: NEC Co., 5-33-1, Shiba, Minatoku, Tokyo 108, Japan.

0021-9991/86 $3.00

restrictions on the grid size using a one-dimensional electromagnetic code including the full dynamics of the particle motions.

We denote the plasma angular frequency as ω_p, a time step as Δt, a grid spacing as Δ, a Debye length as λ_D, and the light speed as c. In conventional plasma simulations, three conditions must be met:

(i) $\Delta \leqslant \lambda_D$,

(ii) $\omega_p \Delta t \leqslant 1$,

(iii) $\Delta t \leqslant \Delta / c$.

The relaxation of the first restriction (i) promises us a significant improvement of the particle simulation for realistic environment: We have many unresolved problems, in which the collective modes with their wavelength much larger than he Debye length λ_D are dominant and the fluctuations with the short wavelength are small enough to be treated as the collisional effects. We have much computational gain, if we succeed in getting high $m_{\text{gain}} = \Delta/\lambda_D$ in the case of the three-dimensional problems. Therefore, some efforts have been done by the many authors. These are reviewed simply in Ref. [6, 7].

Furthermore, it is easily pointed out that the relaxation of the first restriction (i) may help relax the restriction (iii). The time step Δt may be chosen to be the smaller one between $1/\omega_p$ and $(m_{\text{gain}} v_{\text{te}}/c)/\omega_p$, where v_{te} is a thermal speed of the electrons. In the case of a low temperature plasma ($v_{\text{te}}/c \ll 1$), the computational gain on the factor m_{gain} to Δt is clear in addition to the gain to the grid spacing Δ.

Here, we summarize a brief history of the improvement after appearance of CIC–PIC. Abe, Miyamoto, and Itatani [4] have for the first time succeeded in confirming superiority of the higher order spatial interpolation using the quadratic spline and the Fast Fourier Transform (FFT) in the case of $\Delta \geqslant \lambda_D$ and observed a decrease of the total energy error compared with the linear interpolation, when the quadratic spline is used.

Then, Okuda *et al.* [6, 7] challenged to treat the cases of $\lambda_D/\Delta = 0.1 \sim 0.01$ and succeeded in finding its way. They have tested the quadratic spline, cubic spline, and the Gaussian interpolations. Nakajima, Abe, and Itatani [8] applied the quadratic spline to a two-and-one-half, electrostatic dimensional simulation on the wave propagation and plasma heating and have succeeded in treating the large space as an application.

One of purposes of this work is aimed at resolving a problem of treatment of $\lambda_D/\Delta \sim 0.001$. We conclude that the use of the higher order splines is one of the most appropriate methods to reduce the restrictions on the grid size compared with the Debye length for the present digital computer including the so-called super computer such as CRAY in US or VP, S, and SX in Japan. We give an example where the 5th order spline functions have been tested.

As a measure of the reliability of the particle simulation, the total energy error has been usually monitored. At first, its semi-empirical laws on the simulation parameters were obtained by Hockney [9, 10] and Lewis *et al.* [11, 12]. By

introducing rough but useful assumptions, Abe *et al.* [4] succeeded in theoretical analysis, with a scaling law on the temporal fluctuations of the total energy by representing the standard deviation of the total energy error. They introduced the proportional coefficient η inherent to the spatial interpolation scheme. If we find a spatial interpolation with smaller η, this interpolation may be judged as a better from a viewpoint of the accuracy on the conservation of the total energy. In this sense, we now rename η as a model index.

Usually, a self-heating time τ_h introduced by Hockney [9] is used as a measure of accuracy of the total energy error. The meaning of the self-heating time is easily understood. However, it is inconvenient for the cases of the system with little energy error in order to measure directly, because much computer time is thought to be needed. On the other hand, the model index is easily measured as shown in this work, even though the final energy error is very small. The relation of the heating time, τ_h, and the model index η is introduced as $\tau_h \propto 1/\eta^2$ in Ref. [15].

These total energy errors have been shown to be originated by the aliasing error by Langdon [13], however, Abe *et al.* did not clarify the relation between their scaling law and the aliasing error, because their analytical way was difficult to represent the aliasing error explicitly. It is shown in this work that the relation between the scaling law and the aliasing error can be clarified by the modification of the previous work [4].

II. Theoretical Analysis of the Grid Forces

For simplicity, we examine the most basic case: a periodic one-dimensional electrostatic system, which is assumed to be composed of two species of N ions and N electrons and to be charge neutral. The mass and charge densities of the jth particle are m_j and e_j, respectively. In the gridless simulation system, the force F_j acting on the jth particle may be expressed generally[1] by the convolution integral of the weighting function $W(x)$ and the electric field $E(x)$ as

$$F_j = e_j \int_0^L W(x - x_j)\, E(x)\, dx, \tag{1}$$

where L is a period of the system. The physical and the mathematical meaning and figures of the weighting function $W(x)$ will be related to the methods of the spatial interpolations and will be explained later. The equation to the electric field may be given by

$$\begin{aligned} E(x) &= -\frac{d\Phi}{dx}, \\ \frac{d^2\Phi}{dx^2} &= -\frac{1}{\varepsilon_0} \sum_{j=1}^{2N} e_j W(x - x_j). \end{aligned} \tag{2}$$

[1] When the delta function $\delta(x)$ is substituted as $W(x)$, the force is reduced to the usual representation: $F_j = e_j E(x_j)$.

From the periodic boundary condition, the weighting function $W(x)$ is Fourier-expanded as

$$W(x-x_j)=\frac{1}{L}\sum_{m=-\infty}^{\infty} W_m e^{ik_m(x-x_j)}, \qquad k_m=2\pi m/L. \tag{3}$$

Applying Eq. (3) to Eq. (1), we get

$$F_j=\frac{2e_j}{\varepsilon_0 L}\sum_{i=1}^{2N} e_i \sum_{m=1}^{\infty}\frac{W_m^2}{k_m}\sin[k_m(x_j-x_i)]. \tag{4}$$

Now, we introduce the spatial grids on which the physical quantities are numerically calculated and used as the basic quantities of the spatial interpolations for the purpose of saving computer time. We define the weighting function W_g in a gridded system as

$$W_g(x, x_j)=\sum_{l=0}^{M_x-1} W(l\Delta-x_j)\,\delta(x-l\Delta), \tag{5}$$

where M_x is the number of the grids in the system and the grid spacing Δ is L/M_x. This equation may be useful for coding the actual simulation program using the spatial interpolation proposed in this paper.

As a result of the spatial interpolations using the grid quantities, the weighting function W_g, unlike W, in the gridded system cannot be expressed by a function of the differences between the observation point x and the particle point x_j. This causes the Fourier coefficient W_{gm} to be a function of x_j, $W_{gm}=W_{gm}(x_j)$. Therefore, we may Fourier-expand W_g as

$$W_g(x, x_j)=\frac{1}{L}\sum_{m=-M_c}^{M_c} W_{gm}(x_j)\,e^{ik_m(x-x_j)}, \tag{6}$$

where $M_c \leqslant M_x/2$.

This means that the spatial uniformity is lost in the gridded system. In the gridless system or the real space, the spatial uniformity may hold and give a necessary condition for the energy conservation.

The Fourier coefficient $W_{gm}(x_j)$ can be actually calculated as

$$W_{gm}(x_j)=W_m+E_m(x_j), \tag{7}$$

$$E_m(x_j)=\sum_{\substack{n=-\infty \\ n\neq 0}}^{\infty} W_{m+nM_x}e^{-i2\pi n(x_j/\Delta)}, \tag{8}$$

where Eq. (8) is derived in Appendix B.

By comparing Eqs. (6), (7), and (8) with Eq. (3), we may give the gridless weighting function $W(x)$ the physical and mathematical meaning in this paper. In other words, the Fourier coefficient W_m of $W(x)$ for $m \leqslant M_c$ is the averaged value of $W_{gm}(x_j)$ on x_j, when x_j is assumed to be at random distributed. The difference between $W_{gm}(x_j)$ and W_m, $E_m(x_j)$, is sometimes called the aliasing error [13].

Rewriting Eq. (6) by using Eqs. (7) and (8), we can separate the weighting function $W_g(x, x_j)$ in the gridded system into two parts: $W_0(x-x_j)$ with the spatial uniformity and the rest, in a sense error, $E(x, x_j)$ as

$$W_g(x, x_j) = W_0(x-x_j) + E(x, x_j), \tag{9}$$

$$W_0(x-x_j) = \frac{1}{L} \sum_{m=-M_c}^{M_c} W_m e^{ik_m(x-x_j)}, \tag{10}$$

$$E(x, x_j) = \sum_{n=-\infty}^{\infty} W_n(x-x_j)\, e^{-i2\pi n\theta_j}, \tag{11}$$

$$\theta_j = x_j/\Delta - [x_j/\Delta], \tag{12}$$

$$W_n(x-x_j) = \frac{1}{L} \sum_{m=-M_c}^{M_c} W_{m+nM_x} e^{ik_m(x-x_j)}, \tag{13}$$

where the bracket [ ] in Eq. (12) denotes the Gauss notation. The function $W_0(x-x_j)$ is a function which is generated by inverse Fourier expansion of a set of the infinite Fourier coefficient: W_m for $m \leqslant M_c$ and 0 for $m > M_c$.

For the computational convenience, we usually choose $W(x)$, such as it is spatially localized or it vanishes outside of the region with the finite length. On the other hand, $W_0(x)$ is not localized generally.

The function $E(x, x_j)$ is a representation of the aliasing error in real space and is an infinite series whose components are products of the function $W_n(x-x_j)$ with the spatial uniformity and a phase factor representing the differences between the grid point and the particle position.

Using Eq. (7), we can get the force acting on the jth particle in the system:

$$F_{gj} = \frac{2e_j}{\varepsilon_0 L} \sum_{i=1}^{2N} e_i \sum_{m=1}^{M_c} \frac{1}{k_m} [G_{s,m}(x_i, x_j) \sin k_m(x_j - x_i) + G_{c,m}(x_i, x_j) \cos k_m(x_j - x_i)], \tag{14}$$

$$G_{s,m}(x_i, x_j) = [W_m + \varepsilon_m^R(x_i)][W_m + \varepsilon_m^R(x_j)] + \varepsilon_m^I(x_j)\, \varepsilon_m^I(x_i), \tag{15}$$

$$G_{c,m}(x_i, x_j) = \varepsilon_m^I(x_j)[W_m + \varepsilon_m^R(x_i)] - \varepsilon_m^I(x_i)[W_m + \varepsilon_m^R(x_j)], \tag{16}$$

$$\varepsilon_m^R = \mathrm{Re}(E_m),\ \varepsilon_m^I = \mathrm{Im}(E_m). \tag{17}$$

As was done in Ref. [4], we assume the grid forces defined as the difference between the force acting on the particle with the spatially uniform weight

$W_0(x-x_j)$ and the force acting on the particle with the gridded weight $W_g(x, x_j)$. Then, we find

$$\delta F_j = \frac{2e_j}{\varepsilon_0 L} \sum_{i=1}^{2N} e_i \left\{ \sum_{m=1}^{M_c} \frac{1}{k_m} [F_{s,m}(x_i, x_j) \sin k_m(x_j - x_i) + G_{c,m}(x_i, x_j) \cos k_m(x_j - x_i)] \right\}, \tag{18}$$

where

$$F_{s,m}(x_i, x_j) = G_{s,m}(x_i, x_j) - W_m^2. \tag{19}$$

Next, we used the same assumptions as in Ref. [4]. We may summarize them without losing their essence and replace them by a simplified assumption that the positions of the particles are distributed randomly at each time step of the simulation. Then we get the squared value of the standard deviation of the grid forces in the system, $\langle \delta F^2 \rangle$.

$$\langle \delta F^2 \rangle = \left(\frac{4Ne^2}{\varepsilon_0 L}\right)^2 \sum_{m=1}^{M_c} \left(\frac{1}{k_m}\right)^2 \left\{ W_m^2 \sum_{n=1}^{\infty} (W_{m+nM_x}^2 + W_{m-nM_x}^2) + \frac{1}{2}\left[\sum_{n=1}^{\infty} (W_{m+nM_x}^2 + W_{m-nM_x}^2) \right]^2 \right\}. \tag{20}$$

This equation is derived in Appendix C and is confirmed numerically by using the Monte Carlo integration scheme where the particle positions x_i and x_j are taken as uniform random numbers.

In the simulation model using the FFT method, we may adopt the Gaussian filter[2] which reduces the magnitudes of the higher modes in k-space. By the introduction of the characteristic radius R, Eq. (20) is slightly modified as

$$\langle \delta F^2 \rangle = \left(\frac{4Ne^2}{\varepsilon_0 L}\right)^2 \sum_{m=1}^{M_c} \left(\frac{1}{k_m}\right)^2 \left\{ G_m^4 W_m^2 \sum_{n=1}^{\infty} (W_{m-nM_x}^2 + W_{m+nM_x}^2) + \frac{1}{2} G_m^4 \left[\sum_{n=1}^{\infty} (W_{m-nM_x}^2 + W_{m+nM_x}^2) \right]^2 \right\}, \tag{21}$$

$$G_m = \exp\left(-\frac{R^2 k_m^2}{2} \right). \tag{22}$$

[2] In the code, the filtering is done in k-space twice per time step, i.e., at measuring the field quantities and before return to the quantities in real space for calculating the pushing force of each particle. The reader must know that one of reviewers points out that better spatial filter exists than the Gaussian filter. Because any references are not shown, the authors are not sure on this problem but at the moment believe that use of the Gaussian filter is the safest for the subtle simulation parameters from the authors' experiences.

Now, we can estimate the magnitude of the total energy fluctuation due to the grid force. The kinetic energy variation in the system due to the grid force is approximated as [4]

$$\frac{dK_g}{dt} = \sum_{j=1}^{2N} v_j \delta F_j. \tag{23}$$

If δF_j and the particle velocity v_j do not have any correlations, the standard deviation of the temporal derivative of the kinetic energy in the system is evalutated as

$$\sigma^2 \left\{ \frac{dK_g}{dt} \right\} = \langle v^2 \rangle \langle \delta F^2 \rangle, \tag{24}$$

where $\sigma(x)$ denotes a standard deviation of an ensemble x.

Relating this equation with Eq. (21), we can get

$$\sigma^2 \left\{ \frac{dK_g}{dt} \right\} = \frac{1}{\pi} \frac{\mu^2 L^2}{M_x} \omega_p^4 \langle v^2 \rangle \eta^2, \tag{25}$$

where

$$\omega_p^2 = \frac{e^2 N}{\varepsilon_0 \mu L} = \left(\frac{1}{m_i} + \frac{1}{m_e} \right) \frac{e^2 N}{\varepsilon_0 L}, \tag{26}$$

$$\eta^2 = \frac{16\pi}{M_x} \sum_{m=1}^{M_c} \left(\frac{1}{k_m} \right)^2 \left\{ G_m^4 W_m^2 \sum_{n=1}^{\infty} (W_{m-nM_x}^2 + W_{m+nM_x}^2) + \frac{1}{2} G_m^4 \left[\sum_{n=1}^{\infty} (W_{m-nM_x}^2 + W_{m+nM_x}^2) \right]^2 \right\}. \tag{27}$$

Here, the coefficient, i.e., the model index, η is the same as that defined in Ref. [4], but is more general and is represented by the Fourier coefficient of the aliasing error (In Ref. [4], the aliasing error is treated implicitly using the quantities in real space). In the case of $M_c = M_x/2$,[3] the model index η only depends on the model and the cloud radius R.

When M_x is increased to be infinite, η tends to a definite value. If M_x is sufficiently large ($M_x \gg 10$), η is considered to be almost independent of M_x. In other words, η is thought to be determined by the interpolation scheme used in the simulation model, as introduced in Section I.

[3] Throughout this paper, we set as $M_c = M_x/2$.

III. The Properties of the Spline Functions

We define the $(n-1)$th-order spline function $W^{(n)}(x)$ as a function which is obtained by folding the rectangle function with square form $(n-1)$ times by the convolution integral in real space.[4]

Then, their Fourier components in k-space are

$$W_m^{(n)} = \left[\frac{\sin(k_m \Delta/2)}{(k_m \Delta/2)}\right]^n, \tag{28}$$

where $k_m = 2\pi m/L$.

Their forms in real space are shown up to $n=6$ in Fig. 1. As seen easily, $n=1$ corresponds to NGP [1], $n=2$ to CIC–PIC [2, 3], and $n=3$ to the quadratic spline or the modified method 2/2 [4, 6, 7, 8].

These $(n-1)$th-order spline function has the following features:

(a) The higher components in k-space are small.

(b) The 0th mode in k-space does not include the aliasing error and its magnitude is unity, i.e.,

$$\begin{aligned} W_{m+nM_x} &= 1 \quad \text{for} \quad m=0 \text{ and } n=0, \\ &= 0 \quad \text{for} \quad m=0 \text{ and } n\neq 0. \end{aligned} \tag{29}$$

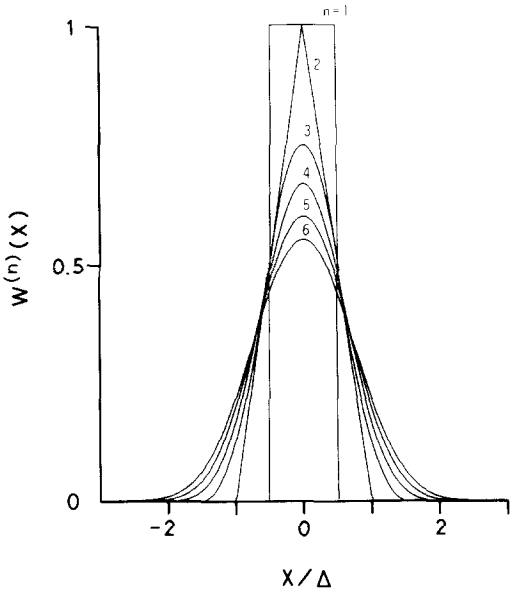

FIG. 1. Form of the spline functions: $W^{(n)}(x)$ for $n=1$ to 6.

[4] The $(n-1)$th-order spline requires n points for charge and current sharing and spatial interpolation of the field quantities. Therefore, we can call the n-point spline for the $(n-1)$th-order spline [15].

This is equivalent to the condition for the charge conservation in the spatial interpolation at any points [13].

(c) In the finite region of real space, their values are finite, i.e.,

$$W(x) \neq 0 \quad \text{for} \quad -n\Delta/2 < x < +n\Delta/2,$$
$$W(x) = 0 \quad \text{for} \quad x \leqslant -n\Delta/2 \text{ and } x \geqslant +n\Delta/2. \tag{30}$$

(d) They are piece-wise polynomials of order $n-1$ in real space and their derivatives are continuous to the $(n-2)$th order. Their actual representations are presented in Appendix A.

(e) The higher order spline function approaches the Gaussian function with the mean value of zero and its standard deviation $\sigma = \Delta(n/12)^{1/2}$. As a result of the spatial smoothing due to use of the higher order spline, this spatial interpolation deteriorates the spatial resolution to the degree which is shown in an example.[5]

Here, we assess the aliasing error by defining the following value:

$$\sigma^2\{E_m^{(n)}\} = \int [E_m^{(n)}(x_j)]^2 \, p(x_j) \, dx_j, \tag{31}$$

where $p(x_j)$ is the probability density and is assumed to be uniform in the system.

The numerical results are presented in Fig. 2 in the cases of $R = 0.0$ and $R = \Delta$. We can see that the aliasing error becomes smaller almost by one order of magnitude, when n is increased by one. Especially, the decreases to the lower modes in k-space are very important, because these modes are physically important and should be retained in the computation.

IV. Comparison between the Model Index η and the Measured Values

Along the scheme explained in Section II, the simulation has been carried out and the value of η is measured up to $n = 6$. The electrons and ions are uniformly set initially. Their velocities form a maxwellian distribution, and their mean value and the thermal speed are adjusted to be exact within each region which is a piece divided to 20 from one period L of the system.

The particles are pushed by the standard leapfrog scheme. The model index η is approximately measured through the calculation of the total energy error. This method is the same as used in Ref. [4] except for the minor improvement explained in the following:

$$\sigma_{\text{exp}}^2 \left\{\frac{dH}{dt}\right\} \cong \frac{1}{N_d} \sum_{i=1}^{N_d} \left(\frac{H_{i+1} - H_i}{\Delta t} - \frac{\Delta H_i}{i\Delta t}\right)^2, \tag{32}$$

[5] For example, σ is about 0.7Δ in the case of $n = 6$. When we use the Gaussian filter with radius $R = \Delta$, the effective radius of the cloud may be approximated to be $(R^2 + \sigma^2)^{1/2} = 1.22\Delta$.

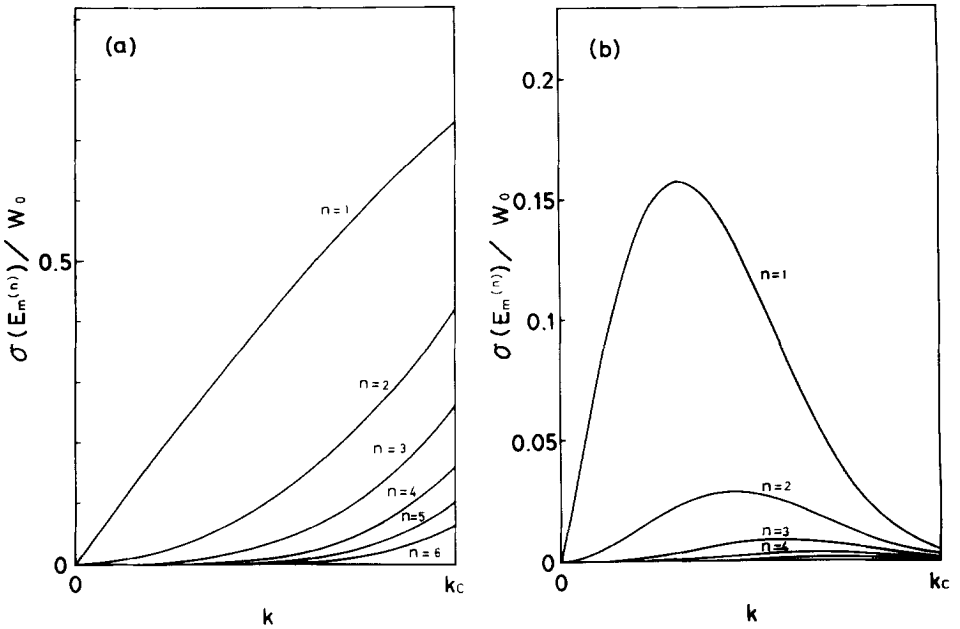

FIG. 2. The magnitudes of the aliasing error for $n=1$ to 6. The ordinate $\sigma\{E_m^{(n)}\}/W_0$ shows the values obtained by dividing by the square root of Eq. (31) by W_0 defined by Eq. (10): (a) for $R=0.0$, (b) for $R=\Delta$, in this case, the graph for $n=6$ is too small to be shown in this scale and is omitted.

where

$$\Delta H_i = H_i - H_0. \tag{33}$$

Then, we get the empirical η from

$$\eta_{\exp} = \frac{(\pi M_x)^{1/2} N}{\omega_p^2 L} \frac{(m_i/\mu)\langle v_i^2\rangle + (m_e/\mu)\langle v_e^2\rangle}{(\langle v_i^2\rangle + \langle v_e^2\rangle)^{1/2}} \sigma_{\exp}. \tag{34}$$

In Fig. 3, both the analytical values of the model index η and their measured values are shown as a function of the radius R of the Gaussian filter. The simulation parameters are $\lambda_D/\Delta = 1.0$, $\omega_p \Delta t = 0.04$, $N=400$, and $m_i/m_e = 100$. The time step is small enough as to avoid the measurement error of $\sigma_{\exp}$ due to the temporal integral. In the usual simulation aimed at the physical study, the longer time step may be recommended from the economical point of view. In any case of n, the measured values are seen to be slightly larger than the analytical values, but their qualitative agreement is said to be quite well in spite of the subtlety of the problem. In Table I, the analytical values of η are presented for $R=0.0$ and $R=\Delta$.

Next, we have measured the model index η as a function of λ_D/Δ between 0.5 and 0.001.

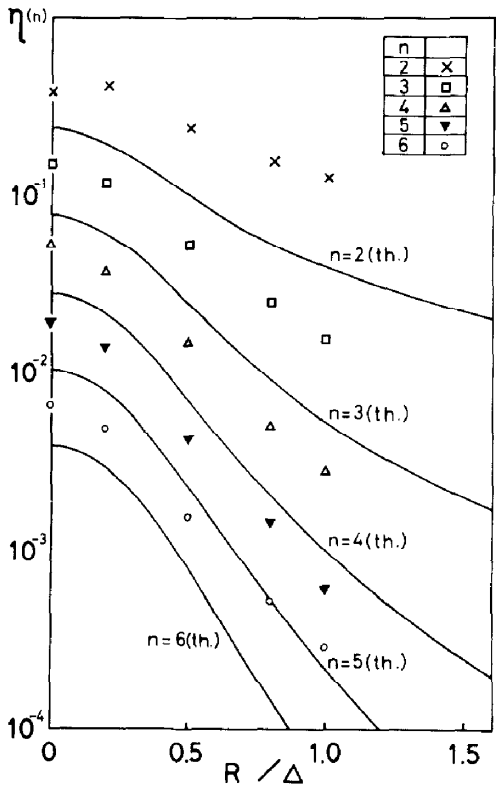

FIG. 3. The analytical model index $\eta^{(n)}$ *vs* R and the measured values for $n = 2$ to 6. These values are calculated from Eq. (27).

TABLE I

The Theoretical Values of the Model Index η for $n = 1$ to 6 with the Radii R of 0.0 and Δ

	η	
n	$R = 0$	$R = \Delta$
1	1.169	5.343×10^{-1}
2	2.437×10^{-1}	4.003×10^{-2}
3	7.818×10^{-2}	5.409×10^{-3}
4	2.786×10^{-2}	9.912×10^{-4}
5	1.032×10^{-2}	2.170×10^{-4}
6	3.900×10^{-3}	5.321×10^{-5}

The simulation parameters are $N=400$ and $=3200$, $m_i/m_e=100$, and $\omega_p T=100$ and 1000, where T is the duration of the simulation run. The time step $\omega_p \Delta t$ is 0.2 except for the case of $\lambda_D/\Delta=0.5$ with a time step $\omega_p \Delta t=0.02$. The minimum total energy error $\Delta H/H$ among runs is so small to be order of 10^{-6}, in a few cases, this small time step is necessary to avoid the situation that the error due to the time integration is larger than that due to the spatial interpolation [4].

The results of the measured η *vs* λ_D/Δ are shown for $R=0.0$ and $R=\Delta$ in Figs. 4a and *b*, respectively, where the horizontal arrows indicate the analytical values. For discussion, we divide them into two parts: the cases of $\lambda_D/\Delta \geqslant 0.07$ and $\lambda_D/\Delta \ll 0.07$. For the former case of $\lambda_D/\Delta \geqslant 0.07$, it can be summarized that the measured values are close to the analytical values. Here, we supplement the following results on the reliability of our theoretical analysis: From the conclusion given in Section II and Ref. 4, the measured $\eta^{(n)}$ should very weakly depend on the grid number M_x and the particle number N, if it is correct. Accordingly, the empirical value $\eta_{\exp}$, which is calculated from N, M_x, other simulation parameters, and $\sigma_{\exp}$ depending on N and M_x (see Eq. (34)), depends only on the model. This theoretical prediction has been already confirmed in Ref. [4] in detail for the case of $\lambda_D \geqslant \Delta$. Again we simply

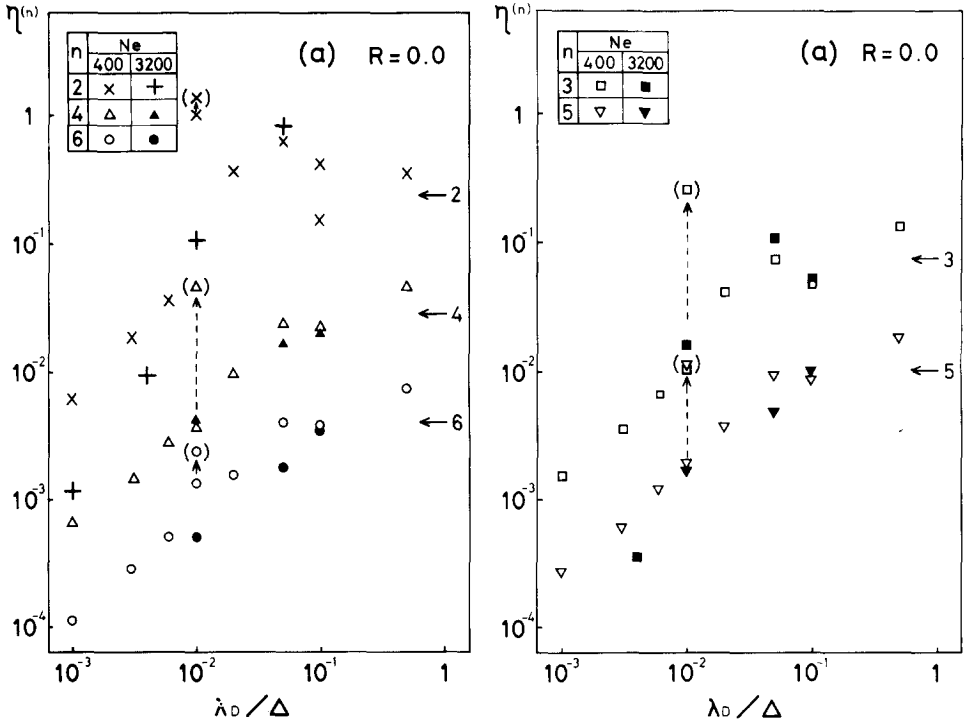

FIG. 4. The measured model index $\eta^{(n)}$ *vs* λ_D/Δ for $n=2$ to 6. These values are calculated from Eq. (34). The horizontal arrows in the right side indicate the analytical values. These values are measured at $\omega_p T=100$ except for those enclosed in the round bracket at $\omega_p T=1000$. The vertical arrows indicate the temporal change of the values between these two time: (a) for $R=0.0$, (b) for $R=\Delta$.

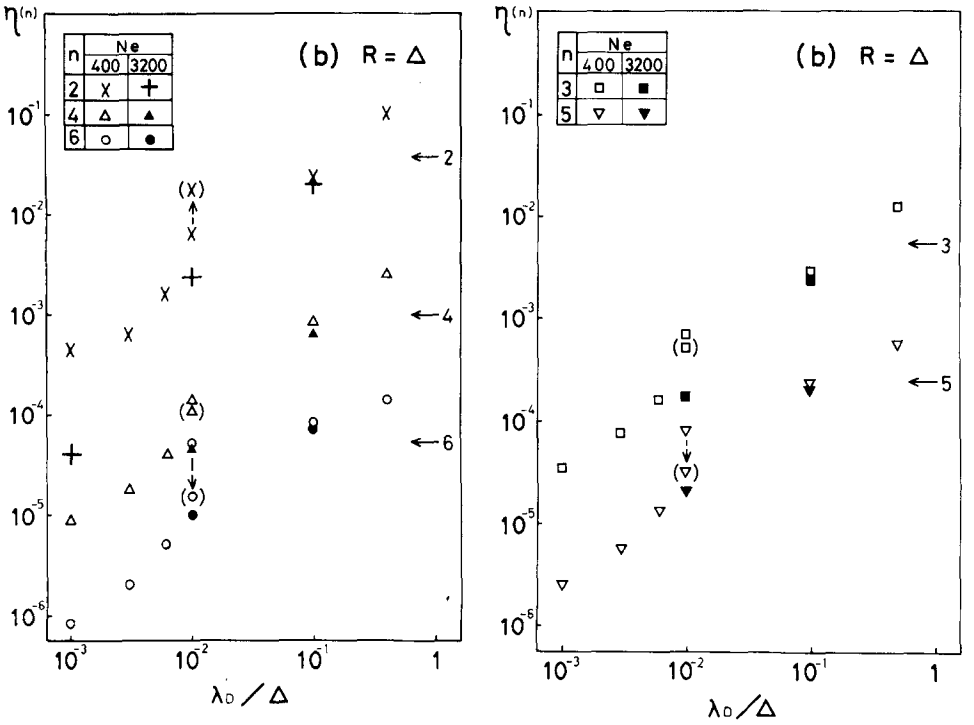

FIG. 4—*Continued.*

confirmed the weak dependence of $\eta_{\exp}$ on N and M_x, where the parameters tested were $M_x = 64$, 128, and 256, and $N = 1600$ within the range of the former case ($\lambda_D/\Delta \geqslant 0.07$).

Then, we discuss on deviation from the theoretical prediction and the smaller measured η compared with the analytical values for the latter case, i.e., $\lambda_D/\Delta \ll 0.07$, as seen clearly in Fig. 4. Anyway, these results may be convenient for the practical uses. We believe the reason lies in the following point: The initial positions of the electrons and ions are the same and are distributed with equal spacing. When λ_D/Δ is small, the regularity of the initial particle distribution persists for a long time. In this case, the assumption required to get Eq. (20) (the position of the particles are distributed randomly at each time step) does not hold. This causes deviation from the theoretical prediction. The grid forces may be cancelled out due to its persisting regularity. Therefore, we observe the smaller η.

Here, we pay attention to the effects of the finite cloud radius, R, for the latter case ($\lambda_D/\Delta = 0.1 \sim 0.01$). In the case of $n = 2$ with $R = 0$ shown in Fig. 4a, the measured η become larger than the analytical values in the comparably early time, $\omega_p T = 100$. In this case, the total energy error $\Delta H/H$ is very large to surpass 100% due to the numerical instability [13]. In Fig. 4, the signs enclosed in the round brackets are the values which are measured at $\omega_p T = 1000$ (ten times longer than

the usual measurement time: $\omega_p T = 100$). Except for the case of $n = 6$, i.e., for the cases of $n = 3$, 4, and 5, with $R = 0.0$, they also surpass beyond the analytical values between $\omega_p T = 100$ and 1000. In these cases, the numerical instability [13] grows after the critical time, the total energy error $\Delta H/H$ surpasses 100% and the measured η becomes larger corresponding to the occurrence of the numerical instability. From these results, we can conclude that the assumptions in analysis of η are broken.

On the other hand, this instability seemed to be stabilized when we used the finite

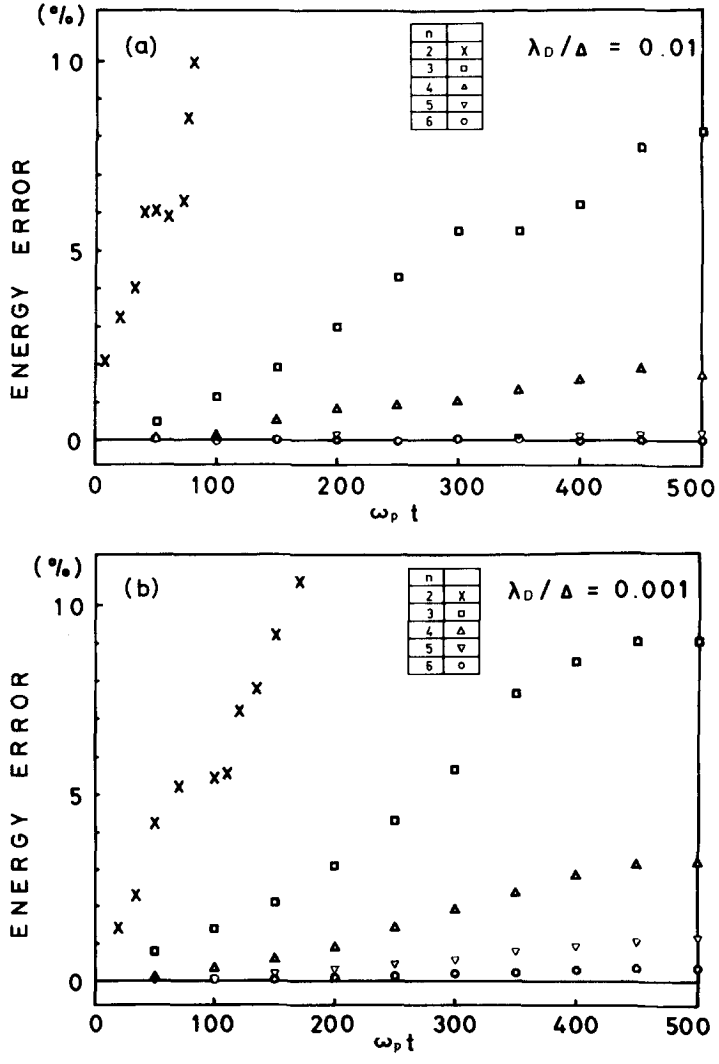

FIG. 5. Total energy error $\Delta H/H_0 = (H - H_0)/H_0$ *vs* $\omega_p T$ for $n = 2$ to 6. The ordinate is shown with percent. (a) for $\lambda_D/\Delta = 0.01$, (b) for $\lambda_D/\Delta = 0.001$.

TABLE II

The Final Energy Errors (%) for $n = 1$ to 6[a]

λ_D/Δ	1	2	3	4	5	6
0.1	$3.213 \times 10^{+3}$	$3.689 \times 10^{+1}$	8.494×10^{-1}	-2.772×10^{-2}	6.244×10^{-3}	2.142×10^{-3}
0.01	$1.770 \times 10^{+5}$	$2.255 \times 10^{+2}$	8.131	1.674	1.665×10^{1}	1.466×10^{-2}
0.001	$1.882 \times 10^{+7}$	$4.568 \times 10^{+1}$	8.897	3.149	1.139	3.685×10^{-1}

Note. $\omega_p t = 500$, $N_e = 400$, $M_x = 32$, $R = \Delta$.

[a] Their temporal changes for $n = 2$ to 6 are shown for $\lambda_D/\Delta = 0.01$ and 0.001 in Figs. 5a and b, respectively.

cloud radius ($R = \Delta$) for the cases of $n \geqslant 3$ with a parameter of $\lambda_D/\Delta = 0.01$. This is consistent with the results presented in Fig. 4b, where we find even the cases that the measured η are decreased from $\omega_p T = 100$ to 1000.

We tried to perform the same test for the cases with $\lambda_D/\Delta = 0.001$ and $R = \Delta$, however, we could not obtain the meaning differences of the results between $\omega_p T = 100$ and 1000.

These all results can be summarized as follows; the runs with the parameters of $\lambda_D/\Delta = 0.01 \sim 0.001$ are stable for a very long time when we use the spline interpolation of $n = 5$ or $n = 6$ with the cloud of the finite size, i.e., $R = \Delta$. It is noted that η is rather decreased from $\omega_p t = 100$ to 1000, when we use these splines in the case of $\lambda_D/\Delta = 0.01$, as seen in Fig. 4b, and therefore we may expect that these splines can keep the same small η in the long time of order of or longer than $\omega_p t = 10000$.

Finally, we choose the typical examples which indicate clearly the results of the improvement done in this work, and show the temporal change of the total errors for the cases of $\lambda_D/\Delta = 0.01$ and 0.001 in Fig. 5. The other simulation parameters are $\omega_p \Delta t = 0.2$, $N = 400$, $m_i/m_e = 100$, $M_x = 32$, and $R = \Delta$. In Table II, we present the final total energy error.

V. Discussion and Conclusion

A series of the spatial interpolation schemes using the higher order splines are proposed and the total energy errors due to their aliasing are theoretically analyzed. We used the model index η as a measure of the accuracy of the model. The model index η was theoretically predicted and compared with the measured values. For a set of parameters ($\Delta \geqslant 0.07\, \lambda_D$), the theoretical predictions agree well with the measured values, if the numerical instability does not grow. In the case of $\Delta \ll 0.07\, \lambda_D$, the measured η is smaller than the theoretical value.[6]

[6] One of reviewers shows an interesting interpretation on this result. Here, we introduce this. Because the number of modes is fixed, the minimum phase velocity supported by the system increases relative to the thermal velocity, as λ_D/Δ decreases. Since $v_{ph} = (3 + 1/k^2\lambda_D^2)^{1/2} v_{th}$, and the maximum value of $k\Delta = \pi$, it follows that the minimum phase velocity is $[3 + \Delta^2/(\pi\lambda_D)^2]^{1/2} v_{th}$. Thus if $\lambda_D/\Delta \leqslant 0.09$, then the minimum phase velocity is larger than 4 v_{th}, and there are no plasma waves in the system which can interact with any electrons. Perhaps this explains the behaviors under and over $\lambda_D/\Delta = 0.07$.

This result is somewhat puzzling at first, however, we believe that the reason lies in violation of the assumption to get Eq. (20) associated with persisting spacial regularity set by the initial condition of our simulation: Almost all the particles oscillate only a fraction of grid space around their positions of free streaming and therefore, the noises, both physical and nonphysical, have not been excited to their thermal level. If the simulation is run much longer than our measurement time ($\omega_p T = 1000$), we have a possibility that the meausered η becomes larger very slowly, even when we use the higher order spline interpolations of $n \geqslant 5$. However, we again ask the reader to pay attention to the note mentioned in the part close to the end of Section IV and add the following fact: we have studied the time-averaged k-spectrum in the thermal plasma using the two dimensional code. We have found a case that the measurement values of the many modes for electrostatic electric field energy reach those calculated using the thermal equilibrium theory at the comparably early time, $\omega_p t = 360$, even in the case of $\lambda_D/\Delta = 0.01$, although they scatter broadly with one order of magnitude (This means that other many modes are under the thermal equilibrium level) and the energy conservation is good in the long time. This study is incomplete and so more work is needed to get the final conclusions of what state the simulation system using the scheme proposed here approaches finally.

In many cases, the time interval in which the numerical noise is sub-thermally excited may persist, as discussed in Section IV. Some readers may be afraid that the physical results may be modified, when $\lambda_D/\Delta \leqslant 0.07$. Actually, the properties of the total energy error are changed. However, this does not necessarily mean that whole the physics changes. In some cases, the low level of noise may be advantageous for a study of various problems of the plasma physics. Such an example was shown in Refs. [8, 14], where the collective wave propagation has been confirmed to be simulated exactly in the case of $\lambda_D/\Delta \cong 0.01$.

Following the examples given in Ref. [6], we tested the cases for a very slow drifting beam. When the splines of $n = 5$ and $n = 6$ were used, all the runs were completely stable and the total energy error were completely negligible for any cases. As a result even the physical two beam instability could not grow to a detectable amplitude within our run time due to the smallness of the initial numerical noise.

In this work, we sometimes used very small time steps in order to measure the total energy error caused only by the spatial grids. From the stability criteria of the leapfrog time integral scheme for the cold plasma, $\omega_p \Delta t$ should be equal or less than 2.0. Actually, the time step of $\omega_p \Delta t = 2.0$ did not cause the numerical instability for the maxwellian plasma with $\lambda_D/\Delta = 0.01$ and 0.001.[7]

We therefore believe a use of a time step close to $\omega_p \Delta t = 1.0$ is not too large in the simulation system when the Debye length is much smaller than the grid size.

[7] Two reviewers pointed out that this fact is unusual. One of them writes that for a thermal plasma, the limit is not 2.0 but 1.63. However, the exact limit is 2.05 in the case of $\lambda_D/\Delta = 0.01$. The energy error at $\omega_p t = 1000$ is 0.15%, when the 5th-order spline ($n = 6$) is used with a parameter of $\omega_p \Delta t = 2.0$. This may be a new discovery. However, it is unstable with parameters of $\lambda_D/\Delta = 1.0$, 0.25 and $\omega_p \Delta t = 2.0$.

The essence of merit for use of the high-order spline is considered to lie in a point: For example, use of the linear spline plus k-space smoothing may not be substituted, as long as the long wave length phenomena are retained in the system. Careful chosen k-space smoothing can reduce the energy error due to the short wave length fluctuations, but the error due to long wavelength fluctuations cannot be reduced, if we use the linear spline.

We should point out that a use of large grid with high-order interpolations reduces the thermal noise and collisions. This happens because the field energy decreases compared with the thermal equilibrium level. This means save of the number of the particles used in the simulation and the substantial save of the simulation cost.

In the strongly magnetized plasma, the phenomena associated with the long wave length ($\lambda \geqslant 100\lambda_D$) are important. The use of the 5th-order spline along the magnetic field and the 2nd-order splines across the field are tested. In this case, the grid points required for the calculation is $3 \times 3 \times 6 = 54$ for the field interpolations, while it is $2 \times 2 \times 2 = 8$ in CIC–PIC. When we use the former interpolation, we can handle space 10^4 times larger or the more than that in CIC–PIC. Therefore, the computational gain is very clear.

Finally, we mention about the cost of use of these weigthings. The discussions for the cost should be separated in two cases: (i) for the present computers such as CRAY, FACOM-VP, HITACHI S-810, and NEC SX, and (ii) for the future computers.

We start from the case (ii). The grid points used for sharing charge or current for a particle are not overlapped, therefore, we may make the computer doing the weigthing of many points for a particle at once. If these computers are realized, we do not need much extra computer time. At the present time (i), we can roughly say that the computer time needed is proportional to the required points for a particle, when VP is used. However, the huge memories and substantial computer time can be saved even in the case of the present computer.

APPENDIX A

We present the forms of the piece-weise polynomials in the spline functions from the zeroth NGP ($n=1$) to the 5th-order ($n=6$). These functions are symmetry on the center of the origin and are given only for $x \geqslant 0$.

〈The 0th order ($n=1$)〉

$$W^{(1)} = \frac{1}{\Delta} \qquad \text{for} \quad 0 \leqslant x \leqslant \frac{\Delta}{2}.$$

〈The 1st order ($n=2$)〉

$$W^{(2)}(x) = \frac{1}{\Delta}\frac{\Delta - x}{\Delta} \qquad \text{for} \quad 0 \leqslant x \leqslant \Delta.$$

⟨The 2nd order $(n=3)$⟩

$$W^{(3)}(x)=\frac{1}{\Delta^3}\left(-x^2+\frac{3}{4}\Delta^2\right) \qquad \text{for} \quad 0\leqslant x\leqslant\frac{\Delta}{2},$$

$$=\frac{1}{\Delta^3}\frac{1}{8}(2x-3\Delta)^2 \qquad \text{for} \quad \frac{\Delta}{2}\leqslant x\leqslant\frac{3}{2}\Delta.$$

⟨The 3rd order $(n=4)$⟩

$$W^{(4)}(x)=\frac{1}{\Delta^4}\frac{1}{6}(4\Delta^3-6\Delta x^2+3x^3) \qquad \text{for} \quad 0\leqslant x\leqslant\Delta,$$

$$=\frac{1}{\Delta^4}\frac{1}{6}(2\Delta-x)^3 \qquad \text{for} \quad \Delta\leqslant x\leqslant 2\Delta.$$

⟨The 4th order $(n=5)$⟩

$$W^{(5)}(x)=\frac{1}{\Delta}\frac{1}{192}\left(115-120\frac{x^2}{\Delta^2}+48\frac{x^4}{\Delta^4}\right) \qquad \text{for} \quad 0\leqslant x\leqslant\frac{\Delta}{2}.$$

$$=\frac{1}{\Delta}\frac{1}{96}\left(55+20\frac{x}{\Delta}-120\frac{x^2}{\Delta^2}+80\frac{x^3}{\Delta^3}-16\frac{x^4}{\Delta^4}\right) \qquad \text{for} \quad \frac{\Delta}{2}\leqslant x\leqslant\frac{3}{2}\Delta.$$

$$=\frac{1}{\Delta}\frac{1}{24}\left(\frac{5}{2}-\frac{x}{\Delta}\right)^4 \qquad \text{for} \quad \frac{3}{2}\Delta\leqslant x\leqslant\frac{5}{2}\Delta.$$

⟨The 5th order $(n=6)$⟩

$$W^{(6)}(x)=\frac{1}{\Delta}\frac{1}{60}\left(33-30\frac{x^2}{\Delta^2}+15\frac{x^4}{\Delta^4}-5\frac{x^5}{\Delta^5}\right) \qquad \text{for} \quad 0\leqslant x\leqslant\Delta.$$

$$=\frac{1}{\Delta}\frac{1}{120}\left(51+75\frac{x}{\Delta}-210\frac{x^2}{\Delta^2}+150\frac{x^3}{\Delta^3}-45\frac{x^4}{\Delta^4}+5\frac{x^5}{\Delta^5}\right) \qquad \text{for} \quad \Delta\leqslant x\leqslant 2\Delta.$$

$$=\frac{1}{\Delta}\frac{1}{120}\left(3-\frac{x}{\Delta}\right)^5 \qquad \text{for} \quad 2\Delta\leqslant x\leqslant 3\Delta.$$

Appendix B: Derivation of Eq. (8)

Normalizing Eq. (3), we get its normalized form as

$$W_N(x-x_j)=\frac{1}{M_x}\sum_{m=-\infty}^{\infty} W_m e^{-ik_m x_j}e^{ik_m x}. \tag{B1}$$

From this equation, we can understand that the Fourier coefficient of $W_N(x-x_j)$ is $W_m e^{-ik_m x_j}$, where the particle locates at $x=x_j$.

Following Eq. (5), $W_N(x-x_j)$ is made sampling on each grid point. Then, its Fourier coefficient is given by the discrete Fourier transform.

$$W_{gm}(x_j)\, e^{-ik_m x_j} = \sum_{l=0}^{M_x-1} W(l\Delta - x_j)\, e^{-ik_m l\Delta}, \tag{B2}$$

where it is noted that $W_{gm}(x_j)$ is a function of x_j.

The R.H.S. equation of Eq. (B2) is calculated as

$$\begin{aligned}
\text{R.H.S.} &= \sum_l \frac{1}{M_x}\left[\sum_{m'=-\infty}^{\infty} W_{m'} e^{ik_{m'}(l\Delta - x_j)}\right] e^{-ik_m l\Delta} \\
&= \frac{1}{M_x}\sum_l \left[\sum_{m'} W_{m'}\, e^{i(k_{m'}-k_m)l\Delta} e^{-ik_{m'}x_j}\right] \\
&= \frac{1}{M_x}\Bigg[\sum_{m' \neq m+nM_x} \sum_l W_{m'} e^{i(k_{m'}-k_m)l\Delta} e^{-ik_{m'}x_j} \\
&\qquad + M_x \sum_{n=-\infty}^{\infty} W_{m+nM_x} \exp(-ik_{m+nM_x}x_j)\Bigg] \\
&= \frac{1}{M_x}\Bigg[\sum_{m'} W_{m'} \frac{1-e^{i(k_{m'}-k_m)M_x\Delta}}{1-e^{i(k_{m'}-k_m)\Delta}} e^{-ik_{m'}x_j} \\
&\qquad + M_x \sum_{n=-\infty}^{\infty} W_{m+nM_x} e^{-ik_m x_j} e^{-i(2\pi M_x/L)nx_j}\Bigg] \\
&= \frac{1}{M_x}\sum_n W_{m+nM_x} e^{-ik_m x_j} e^{-i(2\pi/\Delta)nx_j} \\
&= \left[W_m + \sum_{\substack{n=-\infty \\ n\neq 0}}^{\infty} W_{m+nM_x} e^{-i(2\pi/\Delta)nx_j} e^{-ik_m x_j}\right] e^{-ik_m x_j}.
\end{aligned} \tag{B3}$$

As a result, we get Eq. (8).

Appendix C: Derivation of Eq. (20)

The total grid force δF for the all particles in the system can be expressed by sum of the force ΔF_j acting on the particle j which is given by sum of the force ΔF_{ji} between the particles j and i. Therefore, we get

$$\delta F = \sum_{j=1}^{2N} \Delta F_j = \sum_{j=1}^{2N}\sum_{i=1}^{2N} \Delta F_{ji}. \tag{C1}$$

Considering ΔF_j and ΔF_{ji} as random variables, we can use the theorem of the central limit. As a result, we can relate each standard deviation as

$$\langle \delta F^2 \rangle = 2N \langle \Delta F_j^2 \rangle = (2N)^2 \langle \Delta F_{ji}^2 \rangle. \tag{C2}$$

The grid force ΔF_{ji} can be obtained from Eq. (18),

$$\Delta F_{ji} = \frac{2e_i e_j}{\varepsilon_0 L} \left\{ \sum_{m=1}^{M_c} \frac{1}{k_m} [F_{s,m}(x_i, x_j) \sin k_m(x_j - x_i) + G_{c,m}(x_i, x_j) \cos k_m(x_j - x_i)] \right\}. \tag{C3}$$

Then, we can calculate $\langle \Delta F_{ji} \rangle$ as

$$\langle \delta F_{ji}^2 \rangle = \left(\frac{2e^2}{\varepsilon_0 L} \right)^2 \sum_m \frac{1}{2k_m^2} \langle (G_{s,m} - W_m^2)^2 + G_{c,m}^2 \rangle, \tag{C4}$$

where we have used $\langle \sin^2 k_m(x_j - x_i) \rangle = \langle \cos^2 k_m(x_j - x_i) \rangle = 0.5$. Using the following relations,

$$\begin{aligned} \langle \varepsilon_m^R(x_i)\, \varepsilon_m^I(x_i) \rangle = \langle \varepsilon_m^R(x_i)\, \varepsilon_m^R(x_j) \rangle = \langle \varepsilon_m^I(x_i)\, \varepsilon_m^I(x_j) \rangle = 0, \\ \langle \varepsilon_m^R(x_i) \rangle = \langle \varepsilon_m^I(x_i) \rangle = 0, \end{aligned} \tag{C5}$$

we get Eq. (20).

ACKNOWLEDGMENTS

The authors sincerely acknowledge the reviewers for their useful and interesting comments. One of authors (H.A.) would like to acknowledge that this work has been initiated during his stay in the United States in 1981 under the U.S.–Japan personnel exchange program in the field of the controlled thermonuclear fusion study. H.O. acknowledges the support from the National Science Foundation Grant ATM-8311102 and the Department of Energy Contract DE-AC02-76-CHO-3073 at Princeton University.

REFERENCES

1. R. W. HOCKNEY, *Phys. Fluids* **9** (1966), 1826.
2. R. L. MORSE AND C. W. NIELSON, *Phys. Fluids* **12** (1969), 2418.
3. C. K. BIRDSALL AND D. FUSS, *J. Comput. Phys.* **3** (1969), 494.
4. H. ABE, J. MIYAMOTO, AND R. ITATANI, *J. Comput. Phys.* **19** (1975), 134.
5. W. L. KRUER, J. M. DAWSON, AND B. ROSEN, *J. Comput. Phys.* **13** (1973), 114.
6. H. OKUDA, A. T. LIN, C. C. LIN, AND J. M. DAWSON, *Comput. Phys. Commun.* **17** (1979), 227.
7. H. OKUDA, W. W. LEE, AND C. Z. CHENG, *Comput. Phys. Commun.* **17** (1979), 233.
8. N. NAKAJIMA, H. ABE, AND R. ITATANI, *Phys. Fluids* **25** (1982), 2234.
9. R. W. HOCKNEY, *J. Comput. Phys.* **8** (1971), 19.

10. R. W. HOCKNEY, S. P. GOEL, AND J. W. EASTWOOD, *J. Comput. Phys.* **14** (1974) 148.
11. H. R. LEWIS, A. SYKES, AND J. A. WESSON, *J. Comput. Phys.* **10** (1972), 85.
12. H. R. LEWIS, A. SYKES, AND J. A. WESSON, *J. Comput. Phys.* **13** (1973), 114.
13. A. B. LANGDON, *J. Comput. Phys.* **6** (1970), 247; **12** (1973), 247.
14. H. ABE, *in* "Proceedings of the Topical conference on Radiation in Plasma," Trieste, Italy, June 1983, Vol. 1, p. 177, World Scientific, Republic of Singapore, 1984.
15. C. K. BIRDSALL AND A. B. LANGDON, "Plasma Physics via Computer Simulation," McGraw–Hill, New York, 1985.